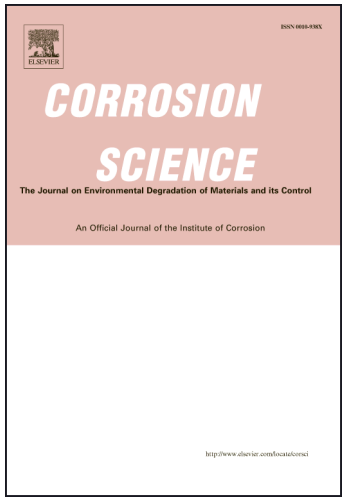

Corrosion and stress corrosion cracking of ultra-high-purity Mg5Zn

Zhiming Shi, Joelle Hofstetter, Fuyong Cao, Peter J Uggowitzer, Matthew S. Dargusch, Andrej Atrens

PII: S0010-938X(15)00043-8
DOI: http://dx.doi.org/10.1016/j.corsci.2015.01.032
Reference: CS 6182

To appear in: *Corrosion Science*

Received Date: 5 December 2014
Accepted Date: 15 January 2015

Please cite this article as: Z. Shi, J. Hofstetter, F. Cao, P.J. Uggowitzer, M.S. Dargusch, A. Atrens, Corrosion and stress corrosion cracking of ultra-high-purity Mg5Zn, *Corrosion Science* (2015), doi: http://dx.doi.org/10.1016/j.corsci.2015.01.032

Corrosion and stress corrosion cracking of ultra-high-purity Mg5Zn

Zhiming Shi[1,2], Joelle Hofstetter[3], Fuyong Cao[1], Peter J Uggowitzer[3], Matthew S. Dargusch[2], Andrej Atrens[1,*]

[1] The University of Queensland, Materials Engineering, School of Mechanical and Mining Engineering, Brisbane, Qld 4072, Australia

[2] The University of Queensland, Centre for Advanced Materials Processing and Manufacturing (AMPAM), Brisbane, Qld 4072, Australia

[3] ETH Zurich, Department of Materials, CH-8093 Zurich Switzerland

* Corresponding author, andrejs.atrens@uq.edu.au, +61 7 3365 3748

Abstract

This paper reports on the measurement of the corrosion rate, and the stress corrosion cracking threshold stress, for ultra-high-purity Mg-5Zn. The corrosion rate was higher than the intrinsic corrosion rate of ultra-high-purity Mg, attributed to the quality of the corrosion product film. The threshold stress for stress corrosion cracking, at an applied stress rate of 0.00016 MPa s^{-1}, was equal to 0.7 times the yield stress in air. The ductility of the cracking indicated that the stress corrosion cracking mechanism was probably hydrogen enhanced localized plasticity.

Keywords: A. Magnesium, B. Weight loss, B. SEM, C. stress corrosion

1. Introduction

Recently, it has become possible to produce some ultra-high-purity (UP) magnesium (Mg) alloys by distillation [1,2,3]. Melt processing in a possible alternative production route for UP Mg alloys [4]. The aim of the present research was to study the corrosion and stress corrosion cracking (SCC) behaviour of one such alloy, UP Mg5Zn.

Magnesium (Mg) is the most active engineering metal, but nevertheless, the corrosion rate of Mg in the atmosphere is lower than that of steels or some aluminium alloys [5,6]. However, the corrosion rates of Mg alloys are higher in aqueous chloride solutions [7,8,9]. This poor corrosion performance in aqueous chloride solutions limits the more widespread use of Mg alloys. The corrosion rate of Mg alloys is typically higher than that of high-purity Mg in aqueous chloride solutions because of micro-galvanic corrosion caused by second phases and Fe-rich particles [5,6,7,8]. The deleterious influence of Fe-rich particles can be overcome in ultra-high-purity Mg, as the Fe content can be lower than that which causes precipitation of Fe-rich particles if the Fe content is greater than the solid solubility, which can be ~ 1 ppm in Mg after heat treatment [10]. Our recent work showed that the intrinsic corrosion rate (as measured by weight loss, P_W) of ultra-high-purity Mg was $P_W = 0.25 \pm 0.7$ mm y^{-1} in 3.5 % NaCl solution saturated with $Mg(OH)_2$ at 25 °C [1,11,12]. Recent work by Hofstetter et al [13] indicated that much lower rates were measured for the ultra-high-purity Mg alloy UPZX50 (Mg-5Zn0.25Ca) using hydrogen evolution. Thus, it is of considerable interest to evaluate the corrosion behaviour of UP Mg5Zn in 3.5% NaCl solution saturated with $Mg(OH)_2$ at 25 °C. This solution has been widely used in our recent research [1,11,12,14,15] so that there is a considerable body of research available for comparison.

Mg alloys also suffer stress corrosion cracking (SCC) [16,17]. SCC can occur at stresses as low as 50% of the yield stress. A continuous second phase along grain boundaries causes intergranular stress corrosion cracking (IGSCC). Heat treatment can dissolve such a

distribution of second phase, and remove the possibility of IGSCC. In contrast, transgranular stress corrosion cracking (TGSCC) can occur in distilled water, indicating that no deleterious ions are needed [18,19,20]. TGSCC involves hydrogen [21]. SCC susceptibility was reported to increase with Zn content [22], although this was disputed by Fairman and Bary [23]. SCC is known to occur in the commercial Mg-Zn alloys ZK60 (6%Zn, <1%Zr) and ZE10 (1%Zn, <1% rare earths) [17] and Choudhary et al [24] found SCC in ZX50 (5%Zn, 0.25%Ca) and WZ21 (2%Y1%Zn) in a synthetic body fluid. Bobby Kannan et al [25] found that ZE41 (4%Zn, 1.19% rare earths) was susceptible to SCC in 0.5 wt.% NaCl solution, and distilled water. Ben-Hamu et al [26] studied the SCC behaviour of Mg-Zn-Mn alloys (6%Zn, 0.5%Mn) containing Si, and found that all alloys were susceptibility to SCC in 3.5% NaCl solution saturated with $Mg(OH)_2$. Cao et al [27] found that Mg5Zn suffered TGSCC in distilled water at low applied stress rate.

Raja and Padekar [28] studied the role of chlorides on pitting and SCC of a wrought Mg2Mn alloy in aqueous chloride solutions. SCC occurred both in the presence and absence of chlorides by a hydrogen embrittlement mechanism. The threshold stress for SCC was estimated to be about 90% of the yield stress in 0.1 M NaCl saturated with $Mg(OH)_2$. Padekar, Raja and Singh Raman [29] found that this alloy had a threshold stress intensity factor for SCC, K_{ISCC}, of 10 MPa $m^{0.5}$ in the same solution compared with a fracture toughness of 15 MPa $m^{0.5}$. Padekar et al. [30] studied the SCC of EV31A in in 0.1 M NaCl solution saturated with $Mg(OH)_2$. The SCC susceptibility of EV31A was lower than that of AZ91E in slow strain rate tests, and EV31A was considered essentially immune to SCC in constant load tests. Padekar et al [31] found that EV31A had a higher threshold stress intensity factor, K_{ISCC}, in the same solution than AZ91A, but a higher stress corrosion crack velocity. Wang et al [32] found that Mg-7%Gd-5%Y-1%Nd-0.5%Zr was susceptible to stress corrosion cracking in 3.5 wt.% NaCl solution.

Thus, it is of interest to evaluate the SCC behaviour of UP Mg5Zn in distilled water.

Thus, the aims of this research were:

1. To evaluate the corrosion behaviour of UP Mg5Zn in 3.5 % NaCl solution saturated with $Mg(OH)_2$.
2. To evaluate the SCC behaviour of UP Mg5Zn in distilled water.

2. Experimental Methods

Specimen material consisted of extruded Mg5Zn, 6 mm in diameter. The Mg5Zn alloy was produced by distillation at the Swiss Federal Institute of Technology Zurich (ETHZ). The ultra-high-purity Mg was produced via vacuum distillation. The purification procedure was performed using a distillation autoclave as described by Löffler et al. [1], Hofstetter et al. [2], and in Cao et al [3]. High-purity graphite crucibles with ash contents of 20 ppm were used to avoid any contamination of the magnesium.

The ultra-high-purity Mg was alloyed with 5 wt.% of zinc (99.999%) in a graphite crucible under a protective gas mixture at 750 °C. The melt was poured into a conical graphite mould with an average diameter of 55 mm and a height of 150 mm. The mould was water cooled at the bottom to avoid shrinkage cavities, and to facilitate directional solidification. The billets were homogenized at 350 °C for 12 h, and cooled with pressurized air.

The homogenized alloy was machined to a billet with a diameter of 50 mm, and a length of 120 mm. Direct extrusion at 320 °C was performed at a ram speed of 0.3 mm/s, to a rod profile with a diameter of 6 mm. This corresponded to an extrusion ratio of 69:1.

Table 1 presents the chemical composition as determined by glow discharge mass spectrometry.

Corrosion testing used fishing-line specimens immersed at the open circuit potential in 3.5 % NaCl aqueous solution saturated with $Mg(OH)_2$ at 25 ± 2 °C for 7 days, as described by Shi and Atrens [33]. This solution has a pH of 10.3 because of the low solubility of $Mg(OH)_2$ as explained in Atrens et al [8], and the pH does not change with test duration. The corrosion rate was evaluated from the evolved hydrogen volume, and from weight loss. Specimen size was 6 mm diameter x 10 mm length. Each surface of each specimen was ground to 2000 grit SiC paper, washed and dried. After the immersion test, corrosion products were removed using chromic acid containing a concentration of CrO_3 of 200 g L^{-1} and 2 g L^{-1} $AgNO_3$. This cleaning solution has been shown to remove corrosion products but no metallic Mg [1,11,12].

The corrosion rate from weight loss, P_W (mm y^{-1}) was determined from [1,11,33]:

$$P_W = 2.1\frac{W_b - W_a}{At_L} \quad (1)$$

where, W_b (mg) is the specimen weight before the immersion test, W_a (mg) is the specimen weight after the immersion test and after removal of corrosion products, A (cm^2) is the surface area of the specimen, and t_L (day) is the immersion duration.

The volume of evolved hydrogen during the immersion test was measured at 25 °C. The average corrosion rate from hydrogen evolution, P_{AH} (mm y^{-1}), was evaluated using [1,11,33]:

$$P_{AH} = 2.088\dot{V}_H \quad (2)$$

where the hydrogen evolution rate, $\dot{V}_H$ (ml cm^{-2} d^{-1}), was evaluated as the total volume of evolved hydrogen per unit area divided by the immersion time. The instantaneous corrosion rate can be evaluated using Eq. (2) and using the instantaneous hydrogen evolution rate.

Stress corrosion cracking (SCC) was studied using the Linearly Increasing Stress Test (LIST) [34] as in our prior studies of the SCC of Mg alloys [18,19,20]. The specimen was

analogous to a tensile specimen with a gauge length of 20 mm and gauge diameter of 5 mm. The specimen, whilst exposed to the solution of interest, (distilled water (DW) in the present study), was subjected to a linearly increasing (engineering) stress until fracture.

The pH of distilled water is initially in the neutral range and slowly increases somewhat due to Mg dissolution. The pH was not measured. A potential drop technique allowed identification of the yield stress (in air or in solution in the absence of SCC), and the threshold stress for SCC in solution. The potential drop technique essentially measures the specimen resistance whilst the (engineering) stress on the specimen is increased at a linear rate. Initially, the specimen resistance increases slowly, and linearly with increasing stress, due to the decrease in specimen gauge section, and the increase in specimen gauge length. There is an acceleration of the rate of increase of specimen resistance when (i) there is stress corrosion crack initiation that significantly decreases the specimen section, or (ii) there is a decreased specimen section due to yielding of the specimen. This allows identification of (i) the SCC threshold stress when there is SCC, or (ii) the yield stress in the absence of SCC.

Two applied stress rates were used: 0.0016 MPa s^{-1} and 0.00016 MPa s^{-1}. These applied stress rates correspond to applied strain rates of 3.6 x 10^{-8} s^{-1} and 3.6 x 10^{-9} s^{-1} in the initial (elastic) portion of the LIST.

3. Results

3.1 Immersion tests

Fig. 1 presents the hydrogen evolution data for Mg5Zn. The volume of evolved hydrogen increased linearly with immersion time for specimen UPMg5Zn-01 for the whole immersion duration, indicating a constant corrosion rate throughout the immersion period. In contrast the volume of evolved hydrogen increased initially linearly for specimen UPMg5Zn-02, but the

rate of increase decreased after 4 days immersion, indicating a decreasing corrosion rate during the second half of the immersion test for specimen UPMg5Zn-02. This second specimen indicated a decreasing hydrogen evolution rate, which was consistent with a partially protective surface film.

Table 2 presents (i) the corrosion rate, P_{AH} (mm y^{-1}), evaluated from the evolved hydrogen volume; and (ii) the corrosion rate, P_W (mm y^{-1}), evaluated from the weight loss. There was agreement between the two independent measures of the corrosion rate, P_{AH} and P_W, although P_{AH} was about 40% smaller than P_W, attributed to some hydrogen dissolving in the Mg specimen as observed previously [1,11,12,]. The average corrosion rate was $P_W = 2.6 \pm 1.2$ mm y^{-1}.

3.2 Stress corrosion cracking

Table 3 presents values of the yield stress, σ_y, for Mg5Zn tested in air, and values of the SCC threshold stress, σ_{SCC}, for Mg5Zn tested in distilled water (DW) using LIST at the nominated applied stress rate. The LISTs in distilled water at an applied stress rate of 0.0016 MPa s^{-1} had values of yield stress, σ_y, or SCC threshold stress, σ_{SCC}, similar to the values of the yield stress, σ_y, in air.

In contrast, the LISTs in distilled water, at an applied stress rate of 0.00016 MPa s^{-1}, had values of the SCC threshold stress, σ_{SCC}, much smaller than the value of the yield stress, σ_y, in air.

Table 3 also presents the values of reduction in area for all LISTs. There was little reduction in area in the tests in air. Furthermore, the reduction in area was similar in distilled water at both the applied stress rates. The LISTs have not been instrumented to allow measurement of specimen strain during the test. Instrumenting to measure strain during the test is difficult, because the gauge section of the specimen is exposed to the solution causing

SCC. The ductility was low in these tests as is evident from the low values of the reduction in area presented in Table 3. This would indicate that the elongation to fracture values would also be low, and moreover, would be expected to be similar in air and in distilled water as were the values of reduction in area. For such low values of elongation to fracture, the errors are large if the elongation to fracture is measured after the test, and so there were no measurements of elongation to fracture.

Fig. 2 presents a typical fracture surface for a specimen fractured in air. The fractography revealed that the surfaces fractured in air had a mixture of ductile dimple rupture features as well as some features that appeared less ductile.

Fig. 3 shows some typical SCC features at the slowest applied stress rate. The SCC regions were at the specimen edge, and extended about 100 μm into the specimen interior, after which there was overload fracture. The SCC features were transgranular and macroscopically brittle. Nevertheless, close inspection indicated some ductile features, consistent with a HELP (hydrogen enhanced localised plasticity) mechanism of SCC.

Fig. 4 presents the typical appearance of an UP-Mg5Zn specimen tested in distilled water at an applied stress rate of 0.0016 MPa s^{-1}. This shows cracks at the surface of the specimen, and distributed evenly on the specimen surface for some distance from the fracture. These surface cracks were consistent with those documented in Fig. 3.

4. Discussion

4.1 Corrosion rates

The average corrosion rate of ultra-high-purity (UP) Mg5Zn, measured by weight loss, was P_W = 2.6 ± 1.2 mm y^{-1}, measured by immersion at the open circuit potential in 3.5 % NaCl solution saturated with $Mg(OH)_2$ at 25 °C. This corrosion rate was somewhat higher

than the intrinsic corrosion rate (as measured by weight loss, P_W) of ultra-high-purity Mg, P_W = 0.25 ± 0.7 mm y^{-1} [3], in the same solution. This indicates that ultra-high-purity by itself is not sufficient to decrease the corrosion rate of a Mg alloy below the intrinsic corrosion rate of high-purity Mg. The fact that the corrosion rate of UP Mg5Zn was greater than that of UP Mg is attributed to the quality of the corrosion product film on the surface of UP Mg5Zn being not as protective as that on UP Mg.

The average corrosion rate of ultra-high-purity (UP) Mg5Zn was P_W = 2.6 ± 1.2 mm y^{-1}. The large error in the measurement of the average corrosion rate was a reflection of the variability of the corrosion rate measurements as is clear from Table 2. This variability was much greater than the measurement errors. For a detailed discussion of measurement errors, please see refs [3,11]. Thus, this variability is intrinsic to the corrosion behaviour of (UP) Mg5Zn. Significant variability was also shown by UP Mg [3] and Mg alloys [11,14]. This indicates that the behaviour of the surface film on the corrosion behaviour of UP Mg, and UP Mg5Zn, has significant variability. This is understandable in view of the fact that the surface film is only partly protective.

4.2 Stress corrosion cracking

The threshold stress for SCC in distilled water at an applied stress rate of 0.0016 MPa s^{-1} was comparable to the yield stress in air. However, the threshold stress for SCC in distilled water at an applied stress rate of 0.00016 MPa s^{-1} was significantly lower than the yield stress in air, 165 MPa compared with 250 MPa. As a ratio, the threshold stress for SCC in distilled water was equal to 0.7 times the yield stress in air. It is highly unlikely that the yield stress changes significantly at these low applied rates, so that it is valid to compare the SCC threshold stress at 0.00016 MPa s^{-1} with the yield stress measured in air at 0.0016 MPa s^{-1}.

Figs. 3 and 4 shows that the stress corrosion cracks occurred at the edge of the specimen as is often the case. These stress corrosion cracks grew until they reached a critical size, and fast fracture ensued.

The SCC morphology was flat, transgranular, and macroscopically brittle, compared with the rest of the fracture surface. Nevertheless, there were signs of ductility, indicating that the SCC mechanism was most probably hydrogen enhanced localized plasticity (HELP), in which hydrogen enhances dislocation mobility, so that a microscopically ductile mechanism leads to a macroscopically brittle process [17].

The fractography indicated, at an applied stress rate of 0.00016 MPa s^{-1}, brittle trangranular SCC initiated at the specimen surface and progressing to a depth of 0.1 mm into the Mg5Zn specimen, whereupon there was a transition to overload fracture. This cracking initiated without the need of any surface pitting, and initiated at a stress considerably below the yield stress. The corrosion tests indicated that the surface film was only partly protective, so it is to be expected that there was corrosion during the LIST, and that the applied stress rate caused additional breaks in the surface film, facilitating corrosion, and hydrogen entry into the Mg5Zn alloy. Moreover, the corrosion studies indicated that the surface film was only partly protective, even in the absence of chloride ions in the solution. This indicates, that whilst chloride ions do facilitate SCC of Mg alloys, chloride ions were not needed for the SCC of Mg5Zn. Distilled water was sufficient to cause stress corrosion cracking of Mg5Zn.

The stress corrosion crack grew to a depth of 0.1 mm into the Mg5Zn specimen, whereupon there was a transition to overload fracture. This is because the LIST is load controlled rather than strain controlled. Fast fracture occurs when the crack length reaches a critical crack size, determined by the fracture toughness of the Mg5Zn.

The applied stress rates of 0.0016 MPa s^{-1} and 0.00016 MPa s^{-1} correspond respectively to applied strain rates of 3.6×10^{-8} s^{-1} and 3.6×10^{-9} s^{-1} in the initial (elastic) portion of the LIST.

These applied stress rates were thus significantly slower than the strain rate of 10^{-6} s^{-1}, which is often used for studying stress corrosion cracking. Testing at a strain rate of 10^{-6} s^{-1}, would not have identified that Mg5Zn is susceptible to stress corrosion cracking in distilled water.

5. Conclusions

1. The average corrosion rate of ultra-high-purity (UP) Mg5Zn, measured by weight loss, was $P_W = 2.6 \pm 1.2$ mm y^{-1}, measured by immersion at the open circuit potential in 3.5 % NaCl solution saturated with $Mg(OH)_2$ at 25 °C. This corrosion rate was somewhat higher than the intrinsic corrosion rate (as measured by weight loss) of ultra-high-purity Mg, P_W = 0.3 mm y^{-1}, in the same solution. The fact that the corrosion rate of UP Mg5Zn was greater than that of UP Mg is attributed to the quality of the corrosion product film on the surface of UP Mg5Zn being not as protective as that on UP Mg.
2. The threshold stress for stress corrosion cracking (SCC) in distilled water of UP Mg5Zn at an applied stress rate of 0.00016 MPa s^{-1} was significantly lower than the yield stress in air, 165 MPa compared with 250 MPa. As a ratio, the threshold stress for SCC in distilled water at an applied stress rate of 0.00016 MPa s^{-1} was equal to 0.7 times the yield stress in air.
3. The SCC facture morphology was flat, transgranular and macroscopically brittle compared with the rest of the fracture surface. Nevertheless, there were signs of ductility, indicating that the SCC mechanism was most probably hydrogen enhanced localized plasticity (HELP).

7. Acknowledgements

The research was supported by the Australian Research Council Centre of Excellence Design of Light Alloys.

Table 1 Chemical composition (in wt% or wt ppm) of the Mg alloy Mg5Zn as determined by glow discharge mass spectrometry.

Alloy	Zn [wt%]	Fe [wt ppm]	Si [wt ppm]	Mn [wt ppm]	Cu [wt ppm]	Ni [wt ppm]
Mg5Zn	4.93	0.17	0.11	1.2	<0.1	<0.01

Table 2 Corrosion rates measured using fishing-line specimens of Mg5Zn immersed at the open circuit potential in 3.5% NaCl aqueous solution saturated with $Mg(OH)_2$ at 25 ± 2 °C for 7 days. The average corrosion rate, P_{AH} (mm y^{-1}), was evaluated from the evolved hydrogen volume; and the average corrosion rate, P_W (mm y^{-1}), was evaluated from the weight loss.

Specimen	P_{AH} (mm y^{-1})	P_W (mm y^{-1})
UP Mg5Zn-01	1.0	1.8
UP Mg5Zn-02	2.3	3.4

Table 3 Values of (i) the yield stress, σ_y, for Mg5Zn specimens tested in air, and values of the stress corrosion cracking threshold stress, σ_{SCC}, for Mg5Zn, tested in distilled water (DW), using LIST at the nominated applied stress rate. Also presented are the values of the reduction in area. The applied stress rates of 0.0016 MPa s^{-1} and 0.00016 MPa s^{-1} correspond respectively to applied strain rates of 3.6 x 10^{-8} s^{-1} and 3.6 x 10^{-9} s^{-1} in the initial (elastic) portion of the LIST.

Specimen	Environment	Applied stress rate, MPa s^{-1}	σ_y or σ_{SCC}, MPa	□□□□□□□ □□□□□□□ □□□, %
01	Air	0.0016	245	2.4
02	Air	0.0016	250	1.3
03	DW	0.0016	247	1.4
04	DW	0.0016	255	2.5
05	DW	0.00016	156	2.0
06	DW	0.00016	174	1.5

References

1 J.F. Löffler, P.J. Uggowitzer, C. Wegmann, M. Becker, H.K. Feichtinger, Process and apparatus for vacuum distillation of high-purity magnesium: European Patent Application PCT/EP 2013/000131 - WO2013/107644, 2012.

2 J. Hofstetter, E. Martinelli, A.M. Weinberg, M. Becker, B. Mingler, P.J. Uggowitzer, J.F. Loffler, Assessing the degradation performance of ultrahigh-purity magnesium in vitro and in vivo, Corros. Sci. 91 (2015) 29-36.

3 F. Cao, Z. Shi, J. Hofstetter, P.J. Uggowitzer, G. Song, M. Liu, A Atrens, Corrosion of ultra-high-purity Mg in 3.5 % NaCl solution saturated with $Mg(OH)_2$, Corros. Sci., 75 (2013) 78-99.

4 A. Prasad, P.J. Uggowitzer, Z. Shi, A. Atrens, Production of high purity magnesium alloys by melt purification with Zr, Adv. Eng. Mater., 14 (2012) 477-490.

5 G. Song, A. Atrens, Corrosion mechanisms of magnesium alloys, Adv. Eng. Mater., 1 (1999) 11-33

6 G. Song, A. Atrens Understanding magnesium corrosion mechanism: a framework for improved alloy performance, Adv. Eng. Mater., 5 (2003) 837-858

7 A. Atrens, M. Liu, NI Zainal Abidin, Corrosion mechanism applicable to biodegradable magnesium implants, Mater. Sci. Eng. B, 176 (2011) 1609-1636.

8 A. Atrens, G.L. Song, F. Cao, Z. Shi, P.K. Bowen, Advances in Mg corrosion and research suggestions, J. Magnesium Alloys, 1 (2013) 177-200.

9 A.Atrens, G.L. Song, M. Liu, Z. Shi, F. Cao, M.S. Dargusch, Review of recent developments in the field of magnesium corrosion, Adv. Eng. Mater., accepted for publication 26 Nov, 2014.

10 M. Liu, P.J. Uggowitzer, A.V. Nagasekhar, P. Schmutz, M. Easton, G. Song, A. Atrens, Calculated phase diagrams and the corrosion of die-cast Mg-Al alloys, Corros. Sci., 51 (2009) 602-619

11 F. Cao, Z Shi, G.L. Song, M. Liu, A. Atrens, Corrosion behaviour in salt spray and in 3.5 % NaCl solution saturated with $Mg(OH)_2$ of as-cast and solution heat-treated binary Mg-X alloys: X = Mn, Sn, Ca, Zn, Al, Zr, Si, Sr, Corros. Sci., 76 (2013) 60-97.

12 Z. Shi, F. Cao, G.L. Song, M. Liu, A. Atrens, Corrosion behaviour in salt spray and in 3.5 % NaCl solution saturated with $Mg(OH)_2$ of as-cast and solution heat-treated binary Mg-RE alloys: RE = Ce, La, Nd, Y, Gd, Corros. Sci., 76 (2013) 98-118

13 J. Hofstetter, M. Becker, E. Martinelli, A.M. Weinberg, B. Mingler, H. Kilian, S. Pogatscher, P.J. Uggowitzer, J.F. Loffler, High-strength low-alloy (HSLA) Mg-Zn-Ca alloys with excellent biodegradation performance, JOM 66(4) (2014) 566-572.

14 Z. Qiao, Z. Shi, N. Hort, N. Zainal Abidin, A. Atrens, Corrosion behaviour of a nominally high purity Mg ingot produced by permanent mould direct chill casting, Corros. Sci., 61 (2012) 185-207.

15 K. Schlüter, Z. Shi, C. Zamponi, F. Cao, E. Quandt, A. Atrens, Corrosion performance and mechanical properties of sputter-deposited MgY and MgGd alloys, Corros. Sci., 78 (2014) 43-54.

16 A. Atrens, N. Winzer, W. Dietzel, Stress Corrosion Cracking of Magnesium Alloys, Adv. Eng. Mater., 13 (2011) 11-18.

17 N. Winzer, A. Atrens, G. Song, E. Ghali, W. Dietzel, K.U. Kainer, N. Hort, C. Blawert, A critical review of the stress corrosion cracking (SCC) of magnesium alloys, Adv. Eng. Mater., 7 (2005) 659-693.

18 N. Winzer, A. Atrens, W. Dietzel, G. Song, K.U. Kainer, Comparison of the Linearly Increasing Stress Test and the Constant Extension Rate Test in the Evaluation of Transgranular Stress Corrosion Cracking of Magnesium, Mater. Sci. Eng. A, 472 (2008) 97-106.

19 N. Winzer, A. Atrens, W. Dietzel, V.S. Raja, G Song, K.U. Kainer, Characterisation of Stress Corrosion Cracking (SCC) of Mg-Al Alloys, Mater. Sci. Eng. A, 488 (2008) 339-351.

20 N. Winzer, A. Atrens, W. Dietzel, G. Song, K.U. Kainer, The Fractography of Stress Corrosion Cracking (SCC) of Mg-Al Alloys, Metal. Mater. Trans. A, 39 (2008) 1157

21 N. Winzer, A. Atrens, W. Dietzel, G. Song, K.U. Kainer, Evaluation of the Delayed Hydride Cracking Mechanism for Transgranular Stress Corrosion Cracking of Magnesium Alloys, Mater. Sci. Eng. A, 466 (2007) 18-31

22 W.K. Miller, Stress-corrosion cracking of magnesium alloys, in: R.H. Jones (Ed.), Stress-Corrosion Cracking: Mater. Perform. Eval., ASM International, Materials Park, (1992) 251-253.

23 L. Fairman, H.J. Bray, Transgranular SCC in Mg-Al alloys, Corros. Sci., 11 (1971) 533-541.

24 L. Choudhary, R.K. Singh Raman, J. Hofstetter, P.J. Uggowitzer, In-vitro characterization of stress corrosion cracking of aluminium-free magnesium alloys for temporary bio-implant application, Mater. Sci. Eng. C, 42 (2014) 629-636.

25 M. Bobby Kannan, W. Dietzel, C. Blawert, A. Atrens, P. Lyon, Stress corrosion cracking of rare-earth containing magnesium alloys ZE41, QE22 and Elektron 21 (EV31A) compared with AZ80, Mater. Sci. Eng. A, 480 (2008) 529-539.

26 G. Ben-Hamu, D. Eliezer, W. Dietzel, K.S. Shin, Stress corrosion cracking of new Mg–Zn–Mn wrought alloys containing Si, Corros. Sci., 50 (2008) 1505-1517.

27 F. Cao, Z. Shi, G. Song, M. Liu, M.S. Dargusch, A. Atrens, Stress corrosion cracking of several solution heat-treated Mg-X alloys, submitted for publication

28 V.S. Raja and B.S. Padekar, Role of chlorides on pitting and hydrogen embrittlement of Mg-Mn wrought alloy, Corros. Sci. 75 (2013) 176-183.

29 B.S. Padekar, V.S. Raja, R.K. Singh Raman, Stress corrosion cracking of a wrought Mg–Mn alloy under plane strain and plane stress conditions, Eng. Fracture Mechan. 102 (2013) 180–193.

30 B.S. Padekar, R.K. Singh Raman, V.S. Raja, P. Lyon, Stress corrosion cracking of a recent rare-earth containing magnesium alloy, EV31A, and a common Al-containing alloy, AZ91E, Corros. Sci. 71 (2013) 1–9.

31 B.S. Padekar, V.S. Raja, R.K. Singh Raman, P. Lyon, Stress corrosion cracking behavior of magnesium alloys EV31A and AZ91E, Mater. Sci. Eng. A 583 (2013) 169–176.

32 S.D. Wang, D.K. Xu, E.H. Han, C. Dong, Stress corrosion cracking susceptibility of a high strength Mg-7%Gd-5%Y-1%Nd-0.5%Zr alloy, J. Magnesium Alloys, (2014), http://dx.doi.org/10.1016/j.jma.2014.11.004.

33 Z. Shi, A. Atrens, An innovative specimen configuration for the study of Mg Corrosion, Corros. Sci., 53 (2011) 226-246

34 A. Atrens, C.C. Brosnan, S. Ramamurthy, A. Oehlert, I.O. Smith. Linearly Increasing Stress Test (LIST) for SCC Research, Meas. Sci. Tech., 4 (1993) 1281-1292

Figure

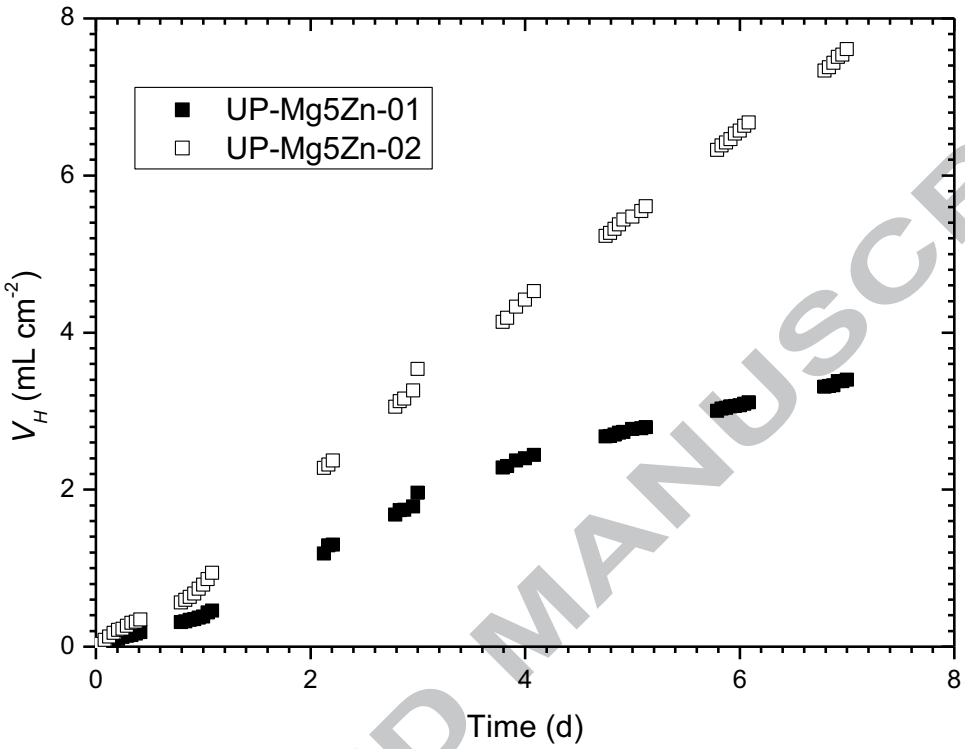

Fig. 1 Hydrogen evolution for UP-Mg5Zn versus immersion time at the open circuit potential in 3.5% NaCl solution saturated with $Mg(OH)_2$.

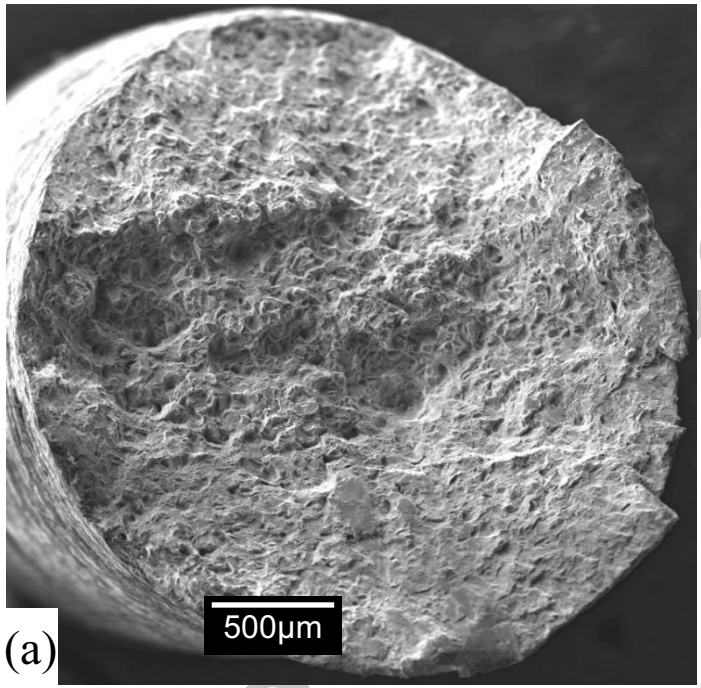

(a)

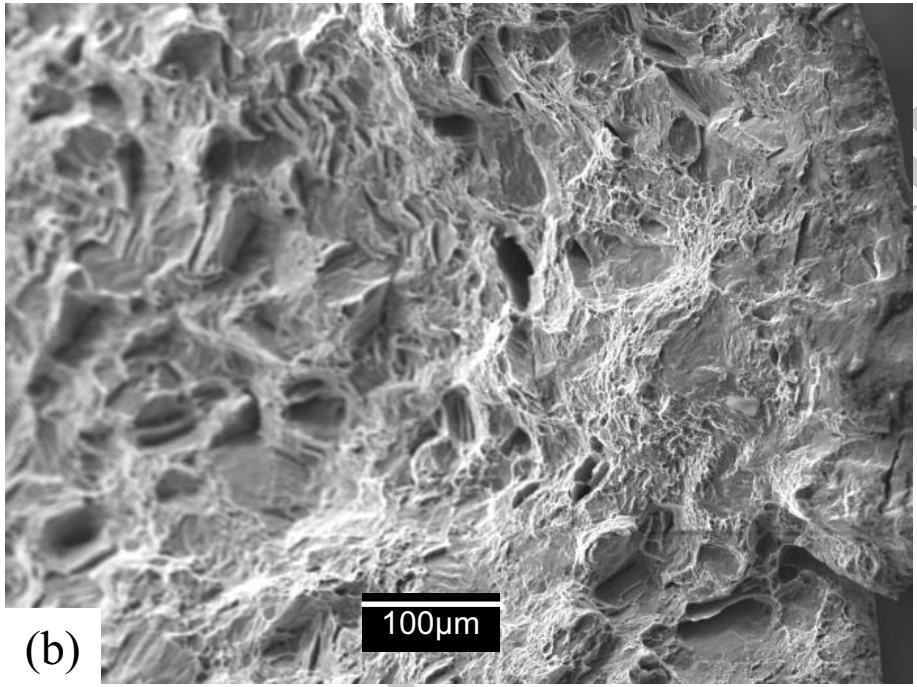

(b)

Fig. 2 Typical fractography for UP-Mg5Zn LIST specimen tested to fracture in air at 25 ˚C at an applied (engineering) stress rate of 0.0016 MPa s^{-1}. In (b) the specimen edge is visible in the top right hand corner. The fractography revealed that the surfaces fractured in air had a mixture of ductile dimple rupture features as well as some features that appeared less ductile. The applied stress rate of 0.0016 MPa s^{-1} corresponds to an applied strain rate of 3.6 x 10^{-8} s^{-1} in the initial (elastic) portion of the LIST.

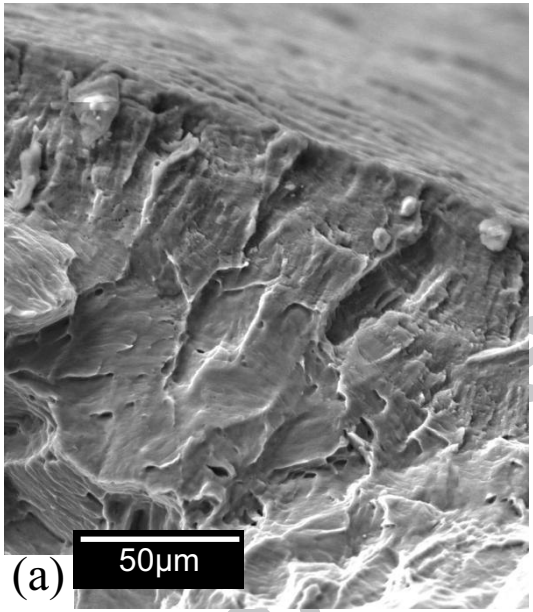

(a)

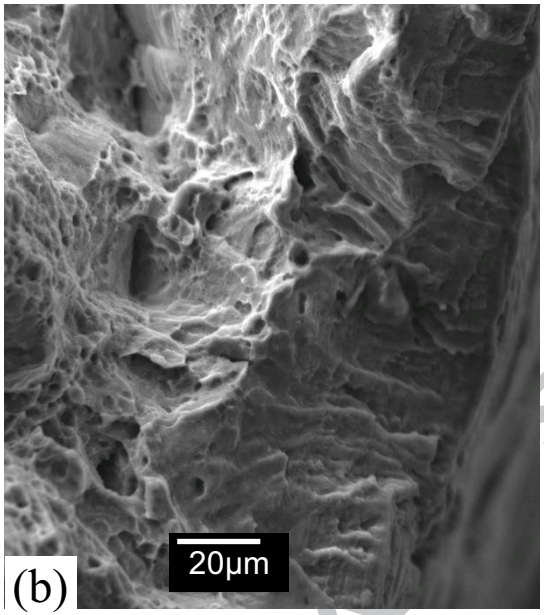

Fig. 3 Typical SEM fractography for UP-Mg5Zn LIST specimen tested to fracture in distilled water at the open circuit potential at 25 ˚C at an applied (engineering) stress rate of 0.00016 MPa s^{-1}. In (a) the specimen edge is visible in the top right hand corner, whereas in (b) the specimen edge is visible in the bottom right hand corner. There was macroscopically flat transgranular SCC fracture at the specimen edge of about 100 µm in depth, and typical dimple rupture in the central area along with brittle features as illustrated in Fig. 2. The applied stress rate of 0.00016 MPa s^{-1} corresponds to an applied strain rate of 3.6×10^{-9} s^{-1} in the initial (elastic) portion of the LIST.

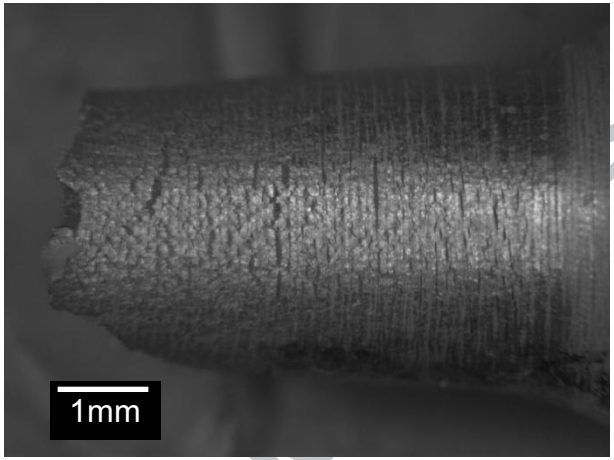

Fig. 4 Typical surface appearance of an UP-Mg5Zn specimen tested in distilled water at 0.0016 MPa s^{-1}, showing numerous surface cracks along the gauge length. Optical micrograph.